

C.O. VANDU<sup>1</sup>  
A.B.M. HEESINK<sup>1</sup>  
G.F. VERSTEEG<sup>1</sup>  
H. BOERRIGTER<sup>2</sup>

<sup>1</sup>Faculty of Science and  
Technology, University of  
Twente, Enschede,  
The Netherlands

<sup>2</sup>Energy Research Center  
of the Netherlands (ECN),  
Petten, The Netherlands

SCIENTIFIC PAPER

66.097.3-039.672:519.87:66.023:  
:57.018.8

## STUDIES ON THE IRON-CATALYZED FISCHER-TROPSCH PROCESS IN A LAMINAR FLOW SLURRY COLUMN REACTOR

*The Fischer-Tropsch process was studied in a laminar flow slurry bubble column reactor. Prior to the experiments, hydrodynamic studies were done in a cold-flow model of the reactor. A mathematical model was also developed for the reactor, based on the kinetic data of an iron-based catalyst. The present modeling approach employed enabled the computation of the extent of gas contraction due to reaction. Six sets of experimental runs were carried out to validate the model, the last utilizing biosyngas, produced by the gasification of willow. The model developed was suitable to predict the performance of the reactor, with the rate parameters adjusted, necessitated by the fact that the catalyst activity changes with time-on-stream. The effect of a number of selected parameters on the Fischer-Tropsch process was also investigated.*

*Key words: Fischer-Tropsch synthesis, Iron catalyst, Slurry bubble column reactor, Mathematical modeling, Experiments, Biomass, Biosyngas.*

Biomass is considered to be the most important renewable energy source for the future (Shell, 2001). When combined with waste-based energy, it currently presents about 3% of the primary energy consumption in the European Union (EU). This share must be tripled within the next decade to fulfill the EU objective of 8.5% energy from biomass and residues by 2010. It is also a prerequisite to enable a reduction of CO<sub>2</sub> emissions as documented in the Kyoto Protocol. An important aspect of biomass is that liquid (bio) fuels can be produced from this renewable source. The emission of CO<sub>2</sub> can be reduced when these 'green' biomass-derived transportation fuels are used in cars, trucks, and buses. One of the most promising routes to produce 'green' fuels is the combination of biomass gasification and Fischer-Tropsch (FT) synthesis. In this route biomass is gasified to yield a biosyngas rich in H<sub>2</sub> and CO. After cleaning, the biosyngas can be used as the feed gas for a FT synthesis reactor where the H<sub>2</sub> and CO are converted into long-chain hydrocarbons that are subsequently converted into 'green diesel' in a post-processing step (Boerrigter et al., 2002).

The production of renewable liquid fuels by a combination of biomass gasification and the FT synthesis is an important research area of the Energy Research Center of the Netherlands (ECN). The research efforts are focused on the cleaning of biosyngas and the effect of the biosyngas composition on the performance of the FT synthesis. One of the experimental facilities applied in this research on the effect of biosyngas on the FT synthesis, is a slurry

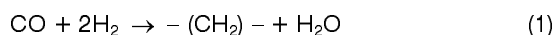
bubble column with an internal diameter of 5.5 cm and a height of 2 m. It has the capability of withstanding operating temperatures as high as 400 °C and a maximum pressure of 40 bar. As a result of its dimensions, operations are carried out in the laminar regime.

The major aim of this paper was the mathematical modeling of this reactor and validation of the model by means of the performed experimental investigations. Two sets of experiments were carried out: the first involving studies on the reactor hydrodynamics and the second, focusing on the conversion of syngas to gaseous and liquid FT products. An understanding of the FT process on a bench-scale provides data for scaling up, a key activity in the commercial operation of the process. Though a number of literature models are available, which can be applied to a bench-scale FT process, none of these model developments have been facilitated by explicit experimental validation, as well as studies on the effects of operating parameters on the FT process.

### REVIEW

#### Fischer-Tropsch Synthesis

In the catalytic FT synthesis, one mole of CO reacts with two moles of H<sub>2</sub> to form mainly aliphatic straight-chain hydrocarbons (C<sub>x</sub>H<sub>y</sub>). About 20% of the chemical energy is released as heat in this exothermic reaction:



As follows from Equation (1), the FT reaction consumes hydrogen and carbon monoxide in a ratio of H<sub>2</sub>/CO = 2. When the ratio in the feed gas is lower, it can be adjusted with the water-gas shift (WGS) reaction:



Paper presented at the 1<sup>st</sup> South-East European Congress of Chemical Engineering, Belgrade, September 25–28, 2005

Author address: G.F. Versteeg, Faculty of Science and Technology, University of Twente, Enschede, The Netherlands  
Email: g.f.versteeg@utwente.nl

Paper received: September 28, 2005  
Paper accepted: May 20, 2006

Typical FT catalysts are based on iron or cobalt. Iron-based catalysts show considerable WGS activity and the  $H_2/CO$  ratio is adjusted in the synthesis reactor. In the case of cobalt-based catalysts, the ratio needs to be adjusted prior to the FT synthesis (Van der Laan, 1999). Typical operating conditions for the FT synthesis are temperatures of 220–280°C and pressures of 25–60 bar. The polymerization-like chain-growth reaction results in a range of products, comprising light hydrocarbons ( $C_1$  and  $C_2$ ), LPG ( $C_3$ – $C_4$ ), naphtha ( $C_5$ – $C_{11}$ ), diesel ( $C_{12}$ – $C_{20}$ ), and wax ( $>C_{20}$ ) fractions. The distribution of the products depends on the catalyst and the conditions under which the process is operated. The chain length distribution can be described by means of the Anderson-Schulz-Flory (ASF) equation with the chain growth probability factor ( $\alpha$ ) as a variable. Higher values of  $\alpha$  give higher molecular weight products. The value of  $\alpha$  is characteristic of the particular catalyst employed in the FT process and catalysts can be tailored towards the production of predominantly low or high molecular weight hydrocarbons (Dry, 1981).

### Literature models

Considerable attention has been given to the use of slurry bubble column reactors for the FT process. The most detailed reviews of reaction engineering models for the slurry FT process are given by Saxena et al. (1986) and Saxena (1995). The earliest models (Calderbank et al., 1963; Satterfield and Huff, 1980; Deckwer et al., 1982; Bukur, 1983) were rather simplified with respect to the species involved by accounting for only  $H_2$ . Recent attempts (Kuo, 1983; Stern et al., 1985; Krishna and Maretto, 1999) have incorporated one or more of the species  $CO$ ,  $CO_2$  and  $H_2O$  with Van der Laan et al. (1999) also taking  $N_2$  into account.

With so many compounds and phenomena that can be taken into account in modeling the FT process, every attempt becomes strongly dependent on inherent assumptions which must be made to enable the unique solution of the governing equations. Two of these assumptions are the particular flow patterns used in representing the gas and liquid (slurry) phases. A number of combinations have been employed by the different investigators. These include modeling both the gas and liquid phases in plug flow (Calderbank et al., 1963; Kuo, 1983), a situation to be encountered in laminar operations, modeling the gas phase in plug flow and the liquid/slurry phase as perfectly mixed (Satterfield and Huff, 1980; Krishna and Maretto, 1999; Van der Laan et al., 1999), as might be obtained in turbulent operations, as well as accounting for axial dispersion in both the gas and liquid phases (Deckwer et al., 1982; Stern et al., 1985). The question here is not about which representation is most accurate but rather which can best be applied to the given process conditions. Turbulent flows are generally encountered in industrial operations and are more attractive from a

commercial point of view (De Swart et al., 1997). Yet, for bench-scale and pilot plant reactors, which are generally several orders of magnitude smaller than industrial reactors, operating in the laminar region is usually applicable in studying the FT process.

When iron-based catalysts are used, both the FT and WGS reactions need to be taken into consideration. A number of investigators have done this (Kuo, 1983; Prakash, 1994; Stern et al., 1985; Stenger and Satterfield, 1985; Inga and Morsi, 1996; Van der Laan et al., 1999). A comparison on the particular kinetic rate expressions used for the FT and WGS reactions has been done (Van der Laan, 1999). Some kinetic investigations tended to separate the derivation of the FT and WGS kinetic expressions by studying them independently. In this way, the interaction of the FT and WGS rates is lost affording less reliable results. It is important that both the FT and WGS expressions be derived from the same set of experimental data using the same catalyst. Of the models in the literature applicable to laminar flow operations, that of Stern et al. (1985) assumed a linear first order rate expression for the FT reaction, which could be misleading (Inga and Morsi, 1996). In most of the performed simulations, the WGS reaction was set at equilibrium making it difficult to understand the relationship between the FT and WGS reactions. The model of Kuo (1983) was developed for the Mobil Corporation and was specifically made to test experimental runs with little emphasis on investigating the effects of operating parameters on the FT process. Areas still open to further investigation, as well as where current literature models are lacking include:

1. Determination of the molar gas contraction due to the conversion of some syngas into liquid products. Where contraction was required in the model equations, a constant value was assumed. Some models accounted for this by incorporating an equation, which traces the change in velocity along the reactor, but did not compute likely molar contraction values.

2. More studies on the effects of operating conditions on mass transfer limitations. Distinctions between  $H_2$  and  $CO$  mass transfer limitations have been made (Inga and Morsi, 1996). Yet, there is a need for a greater understanding of the effect of operating variables on mass transfer. This has not been done for the laminar flow process.

3. Studies on  $CO_2$  inhibition of the process, as well as the presence of  $N_2$  in the feed. Simulations are yet to be available in the literature, which show the effect of  $CO_2$  on reactor performance and how  $CO_2$  may inhibit the FT process. Syngas obtained from either natural gas or biomass gasification may contain small or even large amounts of  $N_2$  and/or  $CO_2$ , depending on the applied gasification conditions and subsequent gas conditioning (i.e.  $CO_2$  removal).

4. The need for a suitable hydrodynamic relationship relating gas hold-up, gas velocity and solids

hold-up. The relationship often utilized (Stern et al., 1985) does not account for the presence of solids in the reaction mixture.

For more general and additional information the interested reader is referred to Bukur and Zimmerman (1987) and Zimmerman and Bukur (1991).

## Physical and Chemical Data

### Kinetic Rate Expression

The kinetic expressions used were derived for a commercially applied, precipitated iron catalyst, Ruhrchemie AG type LP 33/81 (Van der Laan, 1999), basically the same type of catalyst used in the present study.

$$R_{FT} = \frac{k_{FT} P_{CO} P_{H_2}^{1/2}}{(1 + aP_{CO} + bP_{CO_2})^2} \quad (3)$$

$$R_{WGS} = \frac{k_{WGS} (P_{CO} P_{H_2O} - P_{CO_2} P_{H_2} / K_p)}{(P_{CO} + K P_{H_2O})^2} \quad (4)$$

The rate parameter values at 250°C are presented in Table 1. Gas phase component partial pressures on which equations and are based, were converted to the gas phase component concentrations using the ideal

Table 1. Kinetic parameters

Parameter	Value
$k_{FT}$	0.0339 mol kg <sup>-1</sup> s <sup>-1</sup> MPa <sup>-1.5</sup>
$k_{WGS}$	0.0292 mol kg <sup>-1</sup> s <sup>-1</sup>
a	1.185 MPa <sup>-1</sup>
b	0.656 MPa <sup>-1</sup>
K	3.07
$K_p$	85.81

Table 2. Solubility coefficients

Component	Value
H <sub>2</sub>	5.83
CO	4.86
CO <sub>2</sub>	2.32
H <sub>2</sub> O	0.85
N <sub>2</sub>	5.65
C <sub>3</sub> H <sub>8</sub>	5.0*

\*Approximated based on the value for CO<sub>2</sub>

gas relationship. Utilizing the solubility coefficients given in Table 2 (Van der Laan, 1999), the liquid phase component concentrations were thus obtained.

In order to take the effect of temperature on the rate of reaction into account, an Arrhenius temperature dependency was imposed on the FT and WGS rate constants. The activation energy values for the FT and WGS reactions were set at 104 kJ/mol and 125 kJ/mol, respectively (Deckwer et al., 1986; Shen et al., 1994),

and the rate constant data at 250°C (Van der Laan, 1999) were used to derive the pre-exponential factors, resulting in:

$$k_{FT} = 8.27 \times 10^8 \exp(-E_{FT} / RT) \quad (5)$$

$$k_{WGS} = 84 \times 10^{10} \exp(-E_{WGS} / RT) \quad (6)$$

The temperature dependency of the WGS equilibrium constant was obtained from the following relation (Van der Laan, 1999):

$$\log K_p = \log \left( \frac{P_{CO_2} P_{H_2}}{P_{H_2O} P_{CO}} \right)_{eq} = \left( \frac{2073}{T} - 2.029 \right) \quad (7)$$

For more general and additional information the interested reader is referred to Bukur et al. (1995) and Ma et al. (2004).

### Mass Transfer Parameters

The film theory was employed in describing the mass transfer processes that occur in a slurry reactor. To estimate the gas phase mass transfer coefficients, the binary gas phase diffusion coefficients were determined using the method of Fuller, Schettler and Giddings (Reid et al., 1987). For the diffusion of each gas phase component in the multicomponent gas mixture  $D_{G,i}$  the method of Blanc (Reid et al., 1987) was used to determine the diffusion coefficients. The mean bubble diameters were estimated using the correlation of Akita and Yoshida (1974):

$$d_b = 26 d_i \left( \frac{g d_i^3 \rho_L}{\sigma_L} \right)^{-0.5} \left( \frac{g d_i^3}{v_L^2} \right)^{-0.12} \left( \frac{U_G}{\sqrt{g d_i}} \right)^{-0.12} \quad (8)$$

The mean bubble interfacial area is given by:

$$a = 6 \epsilon_G / d_b \quad (9)$$

**For a more system like-relation the reader is referred to Patel et al. (1990).**

The volumetric gas phase mass transfer coefficient at the gas-liquid interface is obtained from:

$$(k_G a)_i = D_{G,i} a / \delta \quad (10)$$

The film theory assumes a gas film thickness,  $\delta$  at the gas-liquid interface where resistance to mass transfer occurs. Though in reality this film does not exist, it serves as a convenient tool in describing mass transfer. It was assumed to be twice the average catalyst particle diameter.

The liquid phase diffusion coefficients for each of the components diffusing into the slurry were estimated using the method of Hayduk and Minhas (Reid et al., 1987). The slurry viscosity was estimated as a function of temperature based on the data available for paraffin wax with an average chain length distribution of 40 carbon atoms. The liquid phase mass transfer coefficients were estimated using the relationship of Stern et al. (1985) whose work was based on the bubble

column mass transfer studies of Shah et al. (1982), which showed that for velocities below  $\sim 5$  cm/s, the volumetric liquid mass transfer coefficient  $k_L a$  was roughly linear with  $U_G$  and used the following correlation for representing  $(k_L a)_{CO}$ :

$$(k_L a)_{CO} = 5 \times 10^{-4} U_G \quad (11)$$

Other component liquid phase mass transfer coefficients were evaluated using the Calderbank and Moo Young correlation (Stern et al., 1985):

$$(k_L a)_i = (k_L a)_{CO} \left[ D_{L,i} / D_{L,CO} \right]^{2/3} \quad (12)$$

The diffusivities have been estimated using the method of Hayduk and Minhas (Reid et al. 1987).

The mass transfer coefficient to the liquid–solid interface was estimated using the correlation of Sano et al. (Beenackers and van Swaaij, 1993), which relates the Sherwood, Reynolds (Re) and Schmidt (Sc) numbers for mass transfer to solid particles in bubble columns:

$$(k_s a_p)_i = (2 + 0.4Re^{0.25}(Sc)_i^{0.33}) (D_{L,i}/d_p) a_p \quad (13)$$

## DEVELOPMENT OF THE REACTOR MODEL

Six components were taken into consideration in modeling the reactor:  $H_2$ ,  $CO$ ,  $CO_2$ ,  $H_2O$ ,  $N_2$  and light hydrocarbons.  $C_3H_8$  (propane) was used to account for the properties of light hydrocarbons, which would generally include hydrocarbons in the range  $C_1$  to  $C_6$ . In the development of a mathematical model for the slurry bubble column reactor, it was assumed that the reactor is operated in the laminar regime. Other assumptions are:

1. The catalyst distribution is uniform throughout the column. This assumption was verified by our experiments (*vide infra*), which show that for small catalyst particles ( $\sim 40 \mu m$ ), sedimentation is unnoticeable even at very low gas velocities.

2. The reactor operates isothermally due to a degree of mixing between the gas and liquid phases.

3. The reactor operates under steady–state conditions and only axial variation in the parameters was considered.

4. The effectiveness factor of the catalyst particles is equal to unity due to the small size of the particles.

5. The hydrodynamic parameters, namely the gas hold–up, diffusion coefficients and solids hold–up were assumed to be spatially independent.

6. The bubble size and gas hold–up are constant throughout the reactor.

## Model Equations

The present study with a cold–flow bubble column reactor facility showed that for velocities below 5 cm/s, laminar flow prevails. The gas bubbles moved along the reactor, in which solid particles were present, in a pattern that approached plug flow, while the slurry phase was slightly back mixed, the degree of mixing increasing with the feed gas velocity. In line with this observation, the slurry bubble column was modeled as comprising of a number of distinct horizontal compartments with the following representation in each compartment: (1) one CISTR for the slurry phase (2) a series of CISTRs for the gas phase. Its characteristic parameters are, therefore, the number of compartments that describe the degree of mixing in the slurry phase,

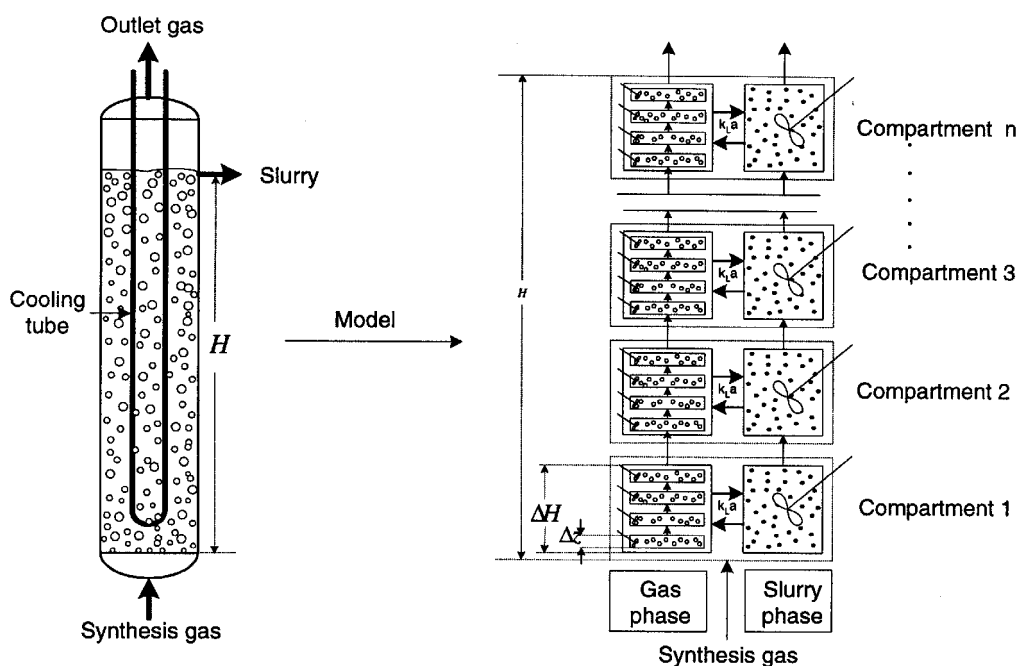


Figure 1. Slurry bubble column reactor model

$n_L$ , as well as that which describes the degree of mixing in the gas phase,  $n_G$ , for a given feed gas velocity. These parameters are approximately related to the slurry and gas phase Bodenstein numbers by (Fogler, 1999):

$$n_L = Bo_L/2 \quad (14)$$

$$n_G = Bo_G/2 \quad (15)$$

The Bodenstein number can be estimated from correlations in the literature (Deckwer, 1992). Figure 1 is a representation of the model for an  $n$ -compartment reactor with a hypothetical four-gas phase CISTR in each compartment. The model is extremely flexible with respect to the degree of mixing in the gas and slurry phases. Its unique structure also permits the determination of gas contraction from one gas phase CISTR to another, making it possible to compute the extent of gas contraction due to the reaction. This is a feature that has not been captured by previous models.

The mass balance for component  $i$  in the completely mixed gas phase is given by:

$$\frac{U_G^{in} C_{G,i}^{in} - U_G^{out} C_{G,i}^{out}}{\Delta z} - (k_L a)_i \left( \frac{C_{G,i}^{out}}{m_i} - C_{L,i}^{out} \right) = 0 \quad (16)$$

while the slurry phase balance for component  $i$  in the completely mixed slurry is:

$$A \int_0^{\Delta H} (k_L a)_i \left( \frac{C_{G,i}^{out}}{m_i} - C_{L,i}^{out} \right) \Delta z + AU_L^{in} C_{L,i}^{in} - AU_L^{out} C_{L,i}^{out} + A \Delta H \varepsilon_L \varepsilon_s \rho_s [\omega_{i,FT} R_{FT} + \omega_{i,WGS} R_{WGS}] = 0 \quad (17)$$

The concentrations are expressed in mol/m<sup>3</sup> and Equation is subject to the boundary condition at the reactor inlet:  $C_{G,i}^{in} = C_{G,i}^{inlet}$ , a specified inlet component gas concentration. The liquid hold-up,  $\varepsilon_L$  is defined as the volume of liquid to the volume of reactor, and the solids hold-up,  $\varepsilon_s$  as the volume of solids to the volume of gas-free slurry.  $\rho_s$  is the catalyst density;  $\omega_{i,FT}$  is the stoichiometric coefficient of component  $i$  in the FT reaction and  $\omega_{i,WGS}$  is the corresponding stoichiometric coefficient of component  $i$  in the WGS reaction. The stoichiometric coefficient of H<sub>2</sub> in the FT reaction was taken to be twice that of CO i.e.  $R_{FT,H_2} = 2 R_{FT,CO}$ .  $m_i$  is the solubility coefficient of  $i$  defined by  $(C_{G,i})_{eq} = m_i (C_{L,i})_{eq}$  with values listed in Table 2. Although the experiments were operated batchwise with respect to the liquid phase, a very small increase was observed in the liquid hold-up in the column due to the production of liquid because of the reaction. This was taken into account in the model via the introduction of a negligible small flowrate through which this increase could be incorporated. In each slurry phase compartment,  $U_L^{in}$  is the inlet slurry superficial velocity, while  $U_L^{out}$  is the outlet slurry superficial velocity, which was set at  $4 \times 10^{-4}$  cm/s as observed from the increase in liquid hold-up in the performed experiments. Correspondingly,  $U_G^{in}$  and  $U_G^{out}$

are the inlet and outlet gas velocities into each gas phase CISTR.

Due to the reaction, the molar flow rate of the gas phase changes. In order to account for this, the superficial gas velocity through the reactor was taken to be a linear function of syngas conversion:

$$U_G^{out} = (1 + \alpha_c) U_G^{inlet} \quad (18)$$

$U_G^{inlet}$  is the inlet gas velocity into the reactor. Assuming there is a total of  $m$  gas phase CISTRs along the reactor height, the gas contraction factor  $\alpha_c$  is defined by:

$$\alpha_c = \frac{\text{Moles of gas of } m \Delta z - \text{Moles of gas into reactor}}{\text{Moles of gas into reactor}} \quad (19)$$

where  $m$  changes from 1 to the total number of gas phase CISTRs. At any given point along the reactor, the syngas conversion is given by:

$$X_{CO+H_2} = \left[ 1 - \frac{(C_{G,H_2}^{out} + C_{G,CO}^{out}) U_G^{out}}{(C_{G,H_2}^{inlet} + C_{G,CO}^{inlet}) U_G^{inlet}} \right] \quad (20)$$

### Hydrodynamic Parameters and Physical Properties

Based on the experiments we carried out (vide infra), the following relationship was derived between the superficial gas velocity into the reactor, the gas hold-up and the solids hold-up.

$$\varepsilon_G = \left( \frac{0.132}{2 + 1.98 \varepsilon_s^{0.3}} \right) U_G^{inlet} (0.97 - 0.32 \sqrt{\varepsilon_s}) \quad (21)$$

The operating pressure has an effect on gas hold-up, which affects the interfacial area of the gas bubbles. This necessitates the correction of Equation, which gives (Krishna and Maretto, 1999):

$$\varepsilon_G = \left( \frac{\rho_G}{\rho_{G,ref}} \right)^{0.48} \left( \frac{0.132}{2 + 1.98 \varepsilon_s^{0.3}} \right) U_G^{inlet} (0.97 - 0.32 \sqrt{\varepsilon_s}) \quad (22)$$

The subscript *ref* refers to ambient conditions (1 bar and 298 K). A number of parameters employed in the development of the model are functions of temperature. These include the gas density, liquid density and liquid viscosity. The gas density of each component was estimated based on the ideal gas law. The mixture density was then computed based on the relative molar amount of gas present. The liquid density and viscosity were made functions of temperature using the relationships given in Equations and . The density of the liquid was based on a linear relationship between the density of the FT wax used for the experiments and temperature. The wax (Parafint C80) had an average molecular weight of 560 g/mol. The viscosity was based on extrapolated data for paraffin wax with an average chain length of 40 carbon atoms.

$$r_L = 900 - 0.64 (T - 273) \quad (23)$$

$$\eta_L = 10^{(932.98 \left( \frac{1}{T} - \frac{1}{461.9} \right))} / 1000 \quad (24)$$

### Numerical Solution Technique

The gas and slurry phase component balances are algebraic equations, the former being linear and the latter non-linear. Thus, the resulting system of equations consists of a mix of linear and non-linear algebraics. A space-marching implementation of the Secant method was adopted to solve the system of equations and an algorithm developed to handle this. The accuracy and stability of the solutions obtained were also investigated. The algorithm developed was implemented in a MATLAB program. It is important to note that the formation of liquid compounds was not taken into account directly in solving the equations. Since only the produced light hydrocarbons are expected to evaporate from the slurry phase, where they are formed in the gas phase, an appropriate stoichiometric coefficient was used to account for the formation of light hydrocarbon products via the FT reaction.

### Model Validation

Model development needs to be facilitated by the validation of the numerical scheme developed. To do this, the case of a simple first order reaction was used. The analytical solution for reactant conversion in this case is given by (Fogler, 1999):

$$X = 1 - 1/(1 + \tau_i k)^n \quad (25)$$

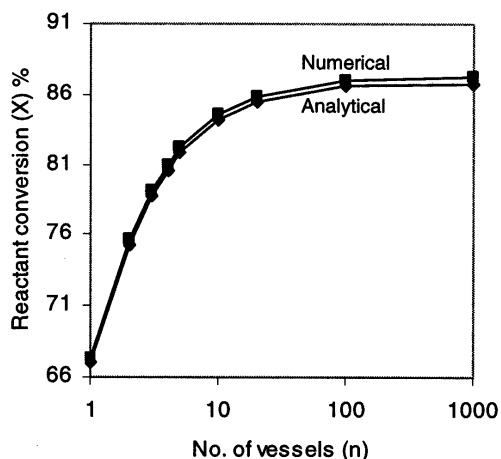


Figure 2. Analytical versus numerical predictions for a first order reaction

Setting the reaction rate group  $\tau_i k$  at 2.03, a comparison of the model-predicted and analytical conversions for a reactant undergoing a first order reaction can be seen in Figure 2. In generating the model-predicted results, equivalent compartments were used for the gas and slurry phases, i.e. each slurry phase compartment corresponded to a single gas compartment. Also, the process was kinetically controlled. This was ensured by the use of a very low catalyst loading value. The result in Figure 2

demonstrates the accuracy and validity of the numerical scheme developed.

### EXPERIMENTAL

In the preparation of the FT experiments, certain factors had to be looked at. These include a study on the hydrodynamics of the reactor in a 'cold-flow' reactor, selection of the suitable FT start-up wax, adequate catalyst preparation, and setting of the operating conditions for the reaction.

#### Cold-Flow Experiments

The need to study the flow patterns in the slurry bubble column was necessitated by the fact that the relationship between the feed gas velocity, solid particle hold-up and gas hold-up had to be established before FT experiments could be carried out. Experiments were carried out in a cold-flow model of the slurry reactor. This model is an exact copy of the reactor, but constructed of glass and operated at ambient temperature and pressure. In all the experiments carried out, air, water and glass pearls were used as the gas, liquid and solid phases, respectively. The glass pearls had a particle size distribution in the range 0–45  $\mu\text{m}$  and 53–106  $\mu\text{m}$  and a skeletal density of 2400  $\text{kg}/\text{m}^3$ . These properties were close enough to those of the iron-based catalyst particles used in the FT experiments, which had a particle size distribution of 0–40  $\mu\text{m}$  and a skeletal density of 1960  $\text{kg}/\text{m}^3$ . The use of water as the liquid phase stemmed from the fact that its viscosity at 25°C and 1 bar was similar to that of the FT wax at 250°C and 15 bar.

Solids hold-up is defined as the volume fraction of solids in the gas-free slurry. Although the glass pearls were not porous, the catalyst particles used for the FT experiment were. In line with the definition of Krishna and Ellenberger (1996), the pore volume of the particles was counted as being part of the solid phase. The slurry height is defined as the combined height of the liquid and solid particles in the reactor. Three different slurry heights were used in conducting the experiments: 0.8, 1.2 and 1.4 m and for each of these heights, the solids hold-up was varied between 0, 10, 20 and 30% of the slurry phase. For each of these solids hold-up in turn, the gas hold-up was determined for inlet superficial gas velocities of 1, 2, 3, 4 and 5  $\text{cm}/\text{s}$ . In this velocity range, the flow in the reactor was homogeneous. At velocities greater than 5  $\text{cm}/\text{s}$ , large bubbles were formed and, due to the small diameter of the reactor, the flow became slugged, that is to say, series of large bubbles were formed, which covered the entire diameter of the reactor.

#### Fischer-Tropsch Experiments

The FT experimental set-up as in operation at the ECN is shown in Figure 3. The reactor has an internal

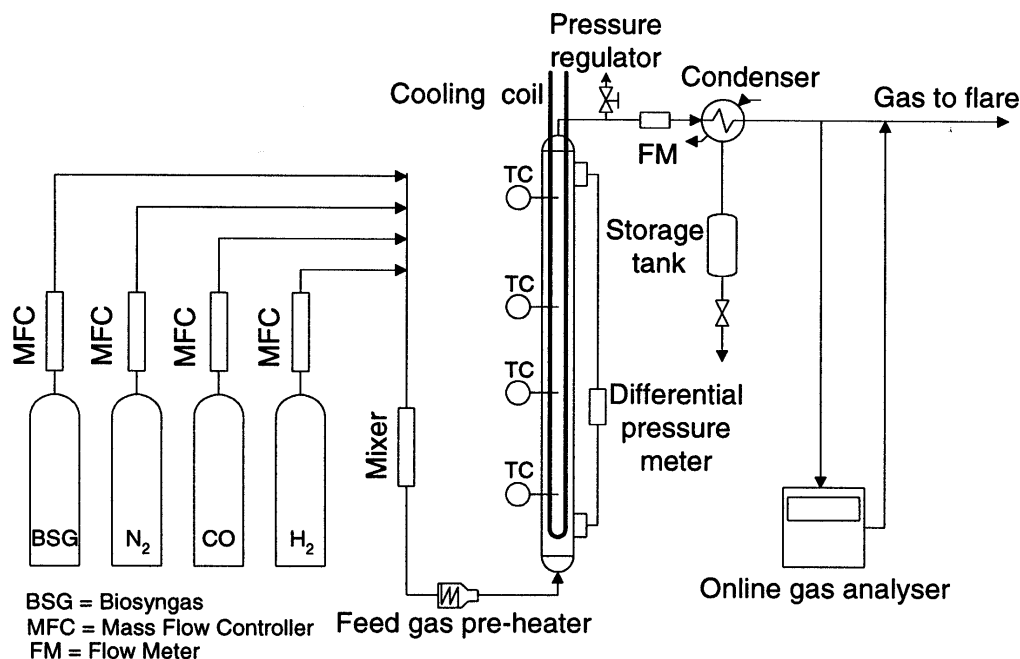


Figure 3. Schematic diagram of the reaction system used for the FT experimental runs

diameter of 5.5 cm with an overall height of 2 m. At its base was a gas distributor plate of the perforated-type design with 49 holes, each with a diameter of 0.5 mm separated by a pitch of 6.5 mm. Constructed on the reactor was a differential pressure meter as an indicator for the increase in the level of the slurry while the reaction proceeded. Four thermocouples were positioned at 0.25, 0.5, 0.75 and 1.75 m along the height of the reactor (measured from the base). The tips of the thermocouples were placed in the heart of the reactor. The lower 1.5 m of the reactor was heated by three independently controlled electrical trace-heating sections to control the reactor temperature. The whole reactor vessel was insulated with glass wool. To enable the removal of excess heat from the exothermic FT reaction, a U-tube cooling coil with an internal diameter of 0.6 cm was used. A standard thermal oil served as the coolant with its temperature kept at approximately 230°C for cooling the reactor. Under start-up conditions, the cooling system was also used to heat up the reactor to above 200°C.

The feed gas was fed from cylinders containing H<sub>2</sub>, CO, N<sub>2</sub>, or biosyngas. The biosyngas was produced by willow gasification and subsequent cleaning of the gas (Boerrigter et al., 2002). Automated mass flow controllers were used to regulate the flow of each of the feed gas constituents into the reactor. The gas was pre-heated to the desired reaction temperature prior to entering the reactor and a gas meter was used to measure the outlet flow rate in order to determine the amount of gas contraction. Unconverted gas was flared. Two gas analyzers were used to analyze the product stream. The first was an online gas analyzer, ABB Advanced Optima capable of detecting the presence of

H<sub>2</sub>, CO, CO<sub>2</sub>, and CH<sub>4</sub>. The second was a gas chromatograph GC 6000 Vega Series and was only used intermittently. It had the capability of analyzing for the presence of C<sub>1</sub> to C<sub>8</sub> hydrocarbons, H<sub>2</sub>, CO, CO<sub>2</sub> and N<sub>2</sub>. The entire experimental set-up was automated and the control system was programmed in WizCon, a software for the automatic control and logging of the process. Online readings of the outlet gas composition, reactor temperature, differential pressure in the reactor, and reactor operating pressure were stored in a database. After the experimental series, a sample of the reactor wax was analyzed off-line. The condensed matter, containing small amounts of aldehydes, alcohols, water, and minor amounts of volatile longer-chain hydrocarbons was not analyzed. In tabulating the results obtained from the experiments, this fraction is reported as "others".

#### Catalyst Preparation and Activation

The catalyst used for the experiments was iron-based and was kindly provided by Celanese (former Ruhrchemie AG), Germany. The particles were crushed and the sieve fraction < 40 µm was calcined under air in an oven at 300°C for 5 hours. Upon calcining, the weight loss of the particles was 8.8%. Before a catalyst can be employed for the FT synthesis, it must be pre-treated to bring it to an active form. While cobalt and nickel catalysts are almost always reduced in flowing H<sub>2</sub> at 200–450°C, to the zero valent metallic state, the purpose for the pre-treatment of iron catalysts is not so clear. Iron catalysts have been pre-treated with H<sub>2</sub>, CO and syngas (Bukur et al., 1989). Moreover, during the FT synthesis, cobalt, nickel and ruthenium catalysts remain in the zero valent state (Anderson, 1984),

whereas iron-based catalysts undergo a change in oxidation states and composition (Dry, 1981; Bukur et al., 1989; Bukur et al., 1995). It is, however, generally agreed that the presence of iron carbides and iron oxide phases are responsible for the activity of iron-based catalysts.

In the present experiments activation was done by the use of CO. The start-up wax, Parafint C80 (a Sasol-Schumann product) (1.6 kg), was introduced into the reactor. The wax was then heated above its congealing point of 80 °C, after which it was left to cool to the ambient temperature of 20 °C. When this had been achieved, 300 g of the crushed and calcined catalyst was introduced into the reactor. This corresponded to an initial solids hold-up  $\epsilon_s$  of 9 vol %. The reactor temperature was then raised from 20 °C to 240 °C by the use of trace heating and the cooling coil. While the reactor was being heated, it was kept under N<sub>2</sub> flow. After heating, the pressure was increased from atmospheric to 6 bar. With the average reactor temperature at 240 °C, the N<sub>2</sub> flow was replaced by the reducing gas, CO. The reaction temperature was then set and maintained at 250 °C, the reduction temperature.

Table 3. Conditions for catalyst activation

Parameter	Value
Operating temperature	250°C
Operating pressure	6 bar
Gas flow rate	18 L <sub>N</sub> /min
Superficial gas velocity	4.1 cm/s
Space velocity	3.79 L <sub>N</sub> /g <sub>cat</sub> .hr
Duration of catalyst activation	17.5 hr

The resulting liquid height in the reactor with the catalyst particles present was approximately 1.17 m. The parameters used for the catalyst activation are given in Table 3. The endothermic nature of the activation reaction meant that the temperature in the reactor had to be kept constant by trace heating. At the conclusion of the catalyst activation process, the CO flow was switched to N<sub>2</sub> and the reactor cooled to 190 °C.

### Experimental FT Runs

In order to begin the FT reaction, the reactor pressure was increased from 6 bar to the desired experimental pressure. The temperature was then gradually raised from 190 °C to 200 °C. At this stage the feed was changed from N<sub>2</sub> to the desired feed gas composition and flow. An overview of the conditions and parameters of the six experiments performed is given in Table 4. The experiments were in principle run to the apparent gas phase steady state (i.e. complete steady state on the catalyst level is not obtained in the relative short test duration), however, in the second and third experiments, complete steady state was not established.

The parameters that were altered between the experiments include the H<sub>2</sub>/CO ratio in the feed, the reaction pressure and the feed gas space velocity. Other variations included the fact that N<sub>2</sub> was incorporated (in the fourth and fifth runs) to mimic the syngas obtained from biomass gasification. The sixth experimental run involved the use of cleaned biosyngas produced at the ECN by the gasification of willow (Boerrigter et al., 2002).

The temperature of the reactor at each thermocouple point, reactor operating pressure, reactor differential pressure, feed gas flow rate, feed gas superficial velocity and the online gas analyzer results were automatically stored in the WizCon database at intervals of one minute. Typically, the volumetric gas contraction (except for the first and second experiments) was recorded when steady state had been reached. During the experiments, the formed liquid and wax products were not removed from the reactor. Therefore, there was a gradual increase in liquid height as the reaction progressed. This change in height corresponded to a change in the differential pressure reading on the reactor. Thus, the readings on the differential pressure meter made it possible for the gradual change in the height of the reactor contents to be followed. At the end of each experimental run, the gas flow was switched to N<sub>2</sub> and the reactor pressure decreased to ~8 bar. In total, the reactor was left running for 144 hours of which 38 hours were spent conducting the six experiments. At other times, it was kept under N<sub>2</sub> flow.

## EXPERIMENTAL RESULTS AND DISCUSSION

### Cold-Flow Experiment Results

The most important results obtained from the cold-flow experiments include:

1. A relationship between the inlet superficial feed gas velocity, solids hold-up and the resulting gas hold-up for the particles of 0–45 μm diameter. The resulting relationship was already given by Equation

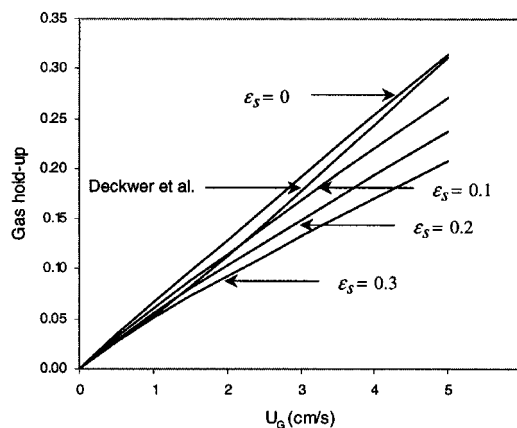


Figure 4. Comparison of the gas hold-up values of Deckwer et al. and the present investigation

(21). This equation is valid for  $U_G^{\text{inlet}}$  ranging from 0 to 5 cm/s where laminar flow predominates and for  $\varepsilon_s$  ranging from 0 to 0.3. The results obtained using Equation (21) were compared to that from the relationship given by Deckwer et al. as quoted by Stern et al. (1984) and are presented in Figure 4. It can be seen that up to superficial gas velocities  $U_G^{\text{inlet}}$  lower than 1 cm/s, the results are practically indistinguishable. However at velocities in excess of 1.5 cm/s, solids hold-up begins to have a noticeable effect on the gas hold-up with the Deckwer et al. correlation over predicting the observed hold-up. Krishna et al. (1997) have also stated the significance of incorporating the effect of the solids concentration on the gas hold-up.

2. The best operating regime of the reactor is the homogeneous or bubble flow regime bordered by a maximum superficial gas velocity of about 5 cm/s. Above this velocity, laminar flow in the reactor transits to slug flow, the latter of which is detrimental to the operation of the reactor since it leads to the formation of large bubbles that simply 'slug' through the reactor leading to a substantial decrease in the residence time of the gas.

3. Low superficial gas velocities are plagued by an uneven distribution of the catalyst particles along the entire height of the reactor. Cold flow studies showed that when particles within the size distribution of 0–45  $\mu\text{m}$  were used, catalyst sedimentation was not

noticeable even at very low superficial gas velocities (< 2 cm/s). However, sedimentation started occurring when the particles of the size range 53–106  $\mu\text{m}$  were used. Thus, catalyst particle sizes had to be as small as possible, preferably below 40  $\mu\text{m}$  for a reactor operated in the laminar regime.

### Fischer-Tropsch Experiment Results

A summary of the results obtained from the FT experiments is given in Table 4. Well over an hour was required for any significant conversion of  $\text{H}_2$  and CO to occur in the first experiment. One reason is that within this time, the temperature of the reactor was being raised from 200°C to the desired 250°C. Even when the reaction progressed to steady state, the syngas conversion value obtained for the operating conditions stood at 40%. The second and third experiments were not conducted to steady state and the data they provide are only indicative. However, the conversions obtained were much higher partly due to the lower superficial gas velocities used and the fact that the  $\text{H}_2/\text{CO}$  feed ratio was the theoretical optimum for obtaining high conversions. The gas contraction values were also higher in comparison to the first experiment, signifying that more of the gaseous feed was converted to liquid products. While quite some time was required before significant conversions occurred in the first experimental run, in the second and third experiments, changes in the

Table 4. Conditions and results for the six test experiments performed

Experimental Runs	1	2	3	4	5	6
Feed gas	Composition (vol%)					
$\text{H}_2$	50	40	40	30	30	bio-syngas <sup>a</sup>
CO	50	60	60	30	30	
$\text{N}_2$	–	–	–	40	40	
$\text{H}_2/\text{CO}$ ratio (–)	1.0	0.67	0.67	1.0	1.0	1.1
Feed gas flow ( $L_n/\text{min}$ )	16.6	13.9	13.9	17.5	29.2	17.3
Initial superficial velocity (cm/s)	1.5	1.2	1.2	1.6	1.6	1.6
Operating pressure (bar)	15	15	15	15	25	15
Space velocity ( $L_n/\text{gcat.hr}$ )	3.5	2.8	2.8	3.7	6.2	3.7
Effective space velocity ( $L_n/\text{gcat.hr}$ ) <sup>b</sup>	3.5	2.8	2.8	2.2	3.7	2.2
Reaction time (hr)	7.3	8.9	8.3	7.0	4.2	4.9
	Results					
Syngas conversion	0.40	0.56	0.55	0.66	0.60	0.57
Gas contraction (%)	25 <sup>c</sup>	33 <sup>c</sup>	33	25	23	22
Off gas	Composition (vol%)					
$\text{H}_2$	44.3	28.2	27.7	20.8	21.2	22.2
CO	36.1	37.5	40.0	6.3	10.3	10.9
$\text{CO}_2$	16.8	27.9	26.1	16.2	13.2	47.7
$\text{N}_2$	0.0	0.0	0.0	53.3	52.0	16.6
$\text{C}_1\text{--C}_6$	1.2	3.2	2.1	1.3	1.0	1.0
Others	1.6	3.2	4.1	2.1	1.3	1.6

<sup>a</sup> The composition of the biosyngas was (in vol%):  $\text{H}_2$  (29), CO (27),  $\text{N}_2$  (1),  $\text{CO}_2$  (32), and Ar (11).

<sup>b</sup> In the reactor 300 g of catalyst were present.

<sup>c</sup> These values were not measured but were estimated from mass balance calculations.

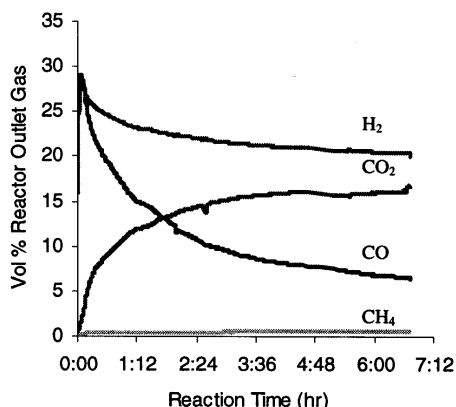


Figure 5a. Gas composition as a function of reaction time for experiment 4

outlet gas concentrations occurred within minutes of commencement. The authors believe that the catalyst was much more activated compared to the first experiment. By the fourth, fifth, and sixth experiments, changes in the concentration profiles were almost immediate on starting the experiments and continued to steady state. The highest conversion was recorded in the fourth experimental run (Figure 5a) where some N<sub>2</sub> was added to the feed to mimic biosyngas (the gas to be used in experiment six, however with CO<sub>2</sub> replaced by N<sub>2</sub>). However, the effective space velocity of this run was relatively low and could account for the high conversion obtained. The fourth and fifth runs were identical except for the fact that the latter was carried out at a higher pressure of 25 bar. For the purpose of comparison, the superficial feed gas velocities, calculated at actual process conditions, in both experiments were similar, meaning that the throughput in the fifth run had to be higher. The higher-pressure process gave a lower conversion.

The sixth experimental run was carried out under the same conditions as the fourth and started with a feed gas mixture consisting of pure N<sub>2</sub>, H<sub>2</sub>, and CO in the ratio 0.45:0.28:0.27 (Figure 5b). When the reaction was observed to be stable (at t = 1.12 hr), the feed was switched over to biosyngas obtained from the gasification of willow. The biosyngas contained 32% CO<sub>2</sub>, and due to this high CO<sub>2</sub> content there was a sudden increase in the amount of CO<sub>2</sub> in the outlet gas of close to 40 vol% immediately after the switch. Due to the presence of the large amount of CO<sub>2</sub>, the reversible WGS reaction equilibrium was shifted more towards the production of CO and H<sub>2</sub>O. The inhibition of the WGS reaction by CO<sub>2</sub> accounts for the lower conversion obtained with biosyngas in comparison to the syngas used in the fourth run, which contained almost the same amount of CO and H<sub>2</sub>. From an analysis of the gaseous hydrocarbons in the sixth experiment, the ASF chain growth probability value (α) was determined to be 0.70.

After the series of six experiments, the reactor wax was analyzed to determine the formation of higher

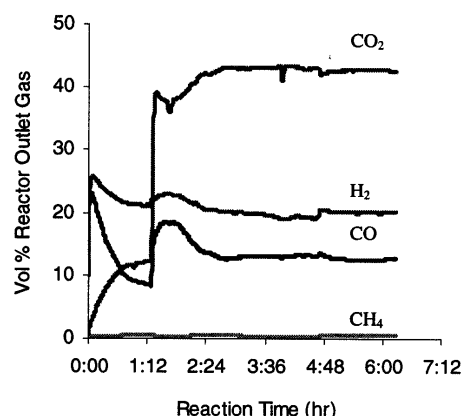


Figure 5b. Gas composition as a function of reaction time for experiment 6

molecular weight non-gaseous hydrocarbons. Hydrocarbons with a chain length up to 100 carbons were detected. Based on the distribution of the C<sub>31</sub>-C<sub>40</sub> products, an average ASF chain growth probability value of α = 0.79 was determined for the heavy hydrocarbons. The observation of two different α-values for the light and heavier hydrocarbons is in agreement with findings in other studies. Evidence for two different chain growth probabilities on iron-based catalysts in the FT synthesis has been reported (Huff and Satterfield, 1984).

## COMPARISON OF MODEL-PREDICTIONS TO EXPERIMENTS

In order to utilize the model developed in predicting the performance of the reactor, its characteristic parameters had to be set. These were the number of gas and liquid phase CISTRs within the range in which the experiments were conducted. For reactors with large aspect ratios the following correlation was proposed (Deckwer, 1992):

$$Bo_G = (2 \times 10^3 \varepsilon_G^2 H) / ((U_G^{inlet})^2 d_t^{1.5}) \quad (26)$$

and from Equation (14),  $n_G = Bo_G/2$ . Similarly, for the slurry phase:

$$Bo_L = U_G^{inlet} H / D_L \quad (27)$$

with the liquid dispersion coefficient obtained from a modified form of the Hikita and Kikukawa equation:

$$D_L = 0.3(0.15 + 0.69(U_G^{inlet})^{0.77}) (d_t^{1.25}) (1/\eta_L)^{0.12} \quad (28)$$

and from Equation (15),  $n_L = Bo_L/2$ . Based on Equations (26) to (28) as well as (14) and (15),  $n_G$  and  $n_L$  were determined to be 50 and 10 approximately, in the range within which the experiments were carried out.

## Correlating Experiments and the Model

Model simulations were run for the same conditions under which the experiments were conducted. A comparison of the model-predicted and

Table 5. Experimental and model-predicted results and model-predicted results with parameters adjusted

Experiment	1		4		5		6	
Reactor height (m)	1.43		1.78		1.86		1.95	
$U_G$ (cm/s)	1.5		1.6		1.6		1.6	
Feed ( $H_2:CO:N_2:CO_2$ )	50:50:0:0		30:30:40:0		30:30:40:0		29:27:12:32	
Pressure (bar)	15		15		25		15	
Solids hold-up	0.09		0.07		0.06		0.06	
Experimental and Model-Predicted Results								
Outlet gas composition	Exp.	Model	Exp.	Model	Exp.	Model	Exp.	Model
$H_2$ (vol%)	44.3	39.6	20.8	23.5	21.2	20.2	22.2	24.1
CO (vol%)	36.1	33.6	6.3	14.1	10.3	19.4	10.9	18.0
$CO_2$ (vol%)	16.8	15.3	16.2	10.8	13.2	5.9	47.7	42.2
$N_2$ (vol%)	0.0	0.0	53.3	49.2	52.0	48.4	16.6	12.6
$C_1-C_6$ (vol%)	1.2	2.1	1.3	1.4	1.0	1.0	1.0	0.7
Others (vol%)	1.6	9.4	2.1	1.0	1.3	5.1	1.6	2.4
Gas contraction	0.25*	0.32	0.25	0.18	0.23	0.17	0.22	0.12
$X_{CO+H_2}$	0.40	0.50	0.66	0.49	0.6	0.46	0.55	0.34
Experimental and Model-Predicted Results with Parameters Adjusted								
Outlet gas composition	Exp.	Model	Exp.	Model	Exp.	Model	Exp.	Model
$H_2$ (vol%)	44.3	43.2	20.8	20.3	21.2	21.9	22.2	20.3
CO (vol%)	36.1	36.3	6.3	6.9	10.3	9.6	10.9	9.7
$CO_2$ (vol%)	16.8	12.9	16.2	15.5	13.2	13.9	47.7	51.1
$N_2$ (vol%)	0.0	0.0	53.3	53.6	52.0	51.8	16.6	15.1
$C_1-C_6$ (vol%)	1.2	1.6	1.3	1.5	1.0	1.3	1.0	1.1
Others (vol%)	1.6	6.0	2.1	2.2	1.3	1.5	1.6	2.7
Gas contraction	0.25*	0.26	0.25	0.25	0.23	0.23	0.22	0.21
$X_{CO+H_2}$	0.40	0.42	0.66	0.66	0.6	0.60	0.55	0.57

\*This value was not measured but was estimated from mass balance calculations

experimental results can be seen in Table 5. With the exception of the first experiment (and ignoring the second and third experiments which were in principle not conducted to steady state), the model affords lower syngas conversion than those obtained from experiments. A large variation in the outlet gas composition of the components can also be seen.

Reports of Bukur et al. (1989) and Davis et al. (1998) indicate that the catalyst activities are clearly dependent on the gas used for activation. The former showed that both in fixed and stirred slurry reactors of laboratory size, CO-activated precipitated iron catalysts gave much higher conversions than  $H_2$ -activated catalysts. In the stirred slurry reactor, syngas conversions after 40 hr of reaction were reported to be 24.8% and 74.8% for the  $H_2$ - and CO-activated catalysts, respectively. However, while the activity of the  $H_2$ -activated catalyst increased with time on stream, that of the CO-activated catalyst decreased. Similar conclusions have also been presented by Davis et al. (1998). An accounting for the change in catalyst activity with time on stream involves adjustment of the values of the FT and WGS rate constants ( $k_{FT}$  and  $k_{WGS}$ , respectively), i.e. fitting of the rate constants, as long as the process is dominantly controlled by chemical

kinetics. As will be shown, this was the case in the range in which the reactor was operated.

### Adaptation of Kinetics

As the model describes the experimental observations correctly in a qualitative manner, the main target of the present study was achieved. However, in adapting the model by fitting it to experimental data, several different parameters can be adapted in order also to arrive at a better quantitative agreement, it was decided to realise this by means of the kinetic constants. This choice was motivated because of the uncertainty in the "true" intrinsic kinetics available in the literature as well as the influences of activation and deactivation during the experiments. Therefore the outcome of the fitting procedure must not be regarded as a kind of

Table 6. Rate constants used to fit the model to the experiments

	F-T rate constant used	WGS rate constant used
Experiment 1	0.7 $k_{FT}$	1.0 $k_{WGS}$
Experiment 4	5.0 $k_{FT}$	5.0 $k_{WGS}$
Experiment 5	2.5 $k_{FT}$	3.0 $k_{WGS}$

determination of the kinetics. The results obtained are given in Table 5. The changes in the FT and WGS rate constants (relative to that used in the model) necessary to obtain the parameter-adjusted model-predicted results given in Table 5 are shown in Table 6 for the first, fourth, fifth, and sixth experimental runs. It can be seen from this that the activity of the catalyst first increased and then began fluctuating with time on stream. The initial increase in activity was due to the fact that the particles were not thoroughly activated at the time the experiments commenced. A decrease in activity with time on stream might be the result of the deposition of carbon on the active sites of the particles caused by the undesired Boudouard side-reaction ( $2\text{CO}$  gives  $\text{C}$  and  $\text{CO}_2$ ). Bukur et al. (1989) also reported the trend of a decrease in catalyst activity with time on stream when the catalyst particles were activated with  $\text{CO}$  as discussed earlier. Acknowledging the fact that the catalyst activity changes with time-on-stream, the model developed can be said to satisfactorily predict the performance of the slurry bubble column reactor for which it was developed. In line with this, the effects of some operating parameters on reactor performance are investigated next.

## NUMERICAL EXPERIMENTS

The reactor model was tested for various operating conditions to study the effects of selected parameters on the FT process. In all the simulations carried out, the physical diameter of the system was restricted to the bench-scale slurry bubble column reactor at the ECN. The superficial gas velocities were restricted to the laminar regime and  $\text{N}_2$  was incorporated in all feeds.  $n_G$  and  $n_L$  were set at 50 and 10, respectively. The effects studied include a variation in the inlet feed gas velocity, catalyst loading, reaction temperature and presence of  $\text{CO}_2$ . Mass transfer and reaction kinetic studies were also carried out.

### Variation in Inlet Feed Gas Velocity

The effect of a change in the feed velocity on the reactor performance was studied within a range of 1 to 5 cm/s. The input parameters for this simulation are given in Table 7. The slurry height refers to the height of the

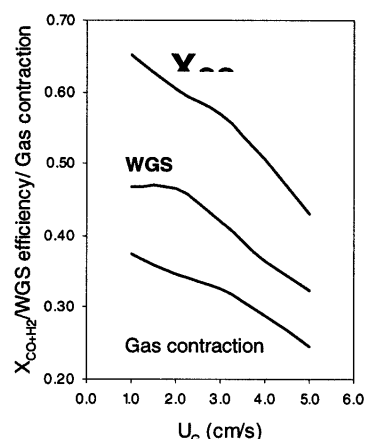


Figure 6. Effect of velocity on syngas conversion, WGS efficiency and gas contraction

liquid and catalyst particles in the reactor prior to the introduction of the feed gas. When gas is introduced into the reactor, this height increases due to the gas hold-up in the slurry. This increase leads to a corresponding increase in the reactor height (note that the term reactor height refers to the combined height of all reacting species in the reactor and not the physical height of the vessel) for a given initial slurry height as well as a decrease in the effective amount of catalyst particles in the reactor.

As shown in Figure 6, for a given solids hold-up, the syngas conversion decreases with an increase in feed gas velocity. Model simulations also show that gas contraction decreases with an increase in the feed velocity. The WGS efficiency, defined as the fraction of  $\text{CO}$  converted which participates in the WGS reaction relative to that which participates in the FT reaction, can also be seen to decrease with an increase in the inlet gas velocity. The reason for this decrease could partly be due to the higher FT kinetic rate constant in comparison to the WGS rate constant at  $250^\circ\text{C}$ .

### Variation in Catalyst Loading

The effect of the amount of catalyst (i.e. the solids hold-up) was investigated. For an initial liquid height of 1 m, catalyst volumes spanning 2, 5, 10, 20, 30 and 40 % of the total slurry volume were used in the

Table 7. Input parameters for the model simulations

	Variables				
	Gas Velocity	Catalyst loading	Temp	Feed Ratio	$\text{CO}_2$
Initial liquid height (m)	1.12	1.0	1.24	Variable	1.38
Initial slurry height (m)	1.40	Variable	1.55	Variable	1.73
Reactor height (m)	Variable	Variable	1.80	2.0	2.0
Feed velocity (cm/s)	Variable	Variable	1.5	Variable	1.5
Catalyst loading (%)	20	Variable	20	20	20
Temp ( $^\circ\text{C}$ )	250	250	Variable	250	250
Feed ratio ( $\text{H}_2$ : $\text{CO}$ : $\text{N}_2$ : $\text{CO}_2$ )	45:45:10:0	45:45:10:0	45:45:10:0	Variable	Variable
Pressure (bar)	15	15	15	15	15

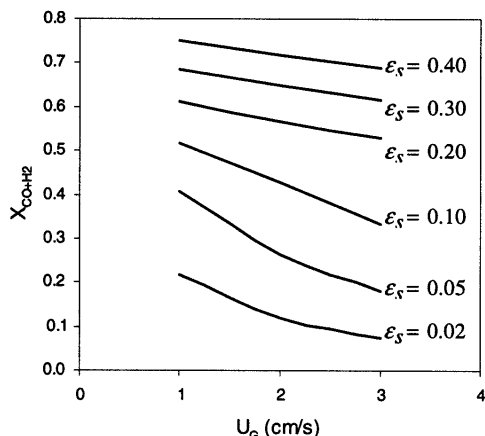


Figure 7. Effect of catalyst loading on syngas conversion at different feed velocities

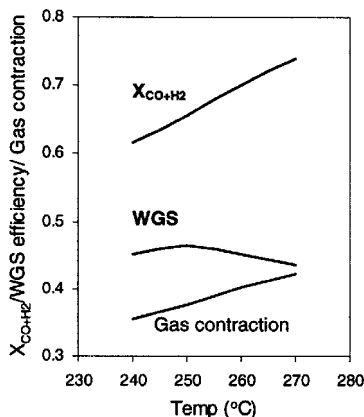


Figure 8. Effect of temperature on syngas conversion, WGS efficiency and gas contraction

simulations. The feed velocities were also altered within a range of 1 to 3 cm/s to see what effect they have on conversion with respect to the amount of catalyst in the reactor. Input data for the simulations are given in Table 7 and the results obtained in Figure 7. Higher amounts

of catalyst in the reactor give rise to higher conversions of syngas. Though larger solid hold-ups may be desirable, they also tend to cause small bubbles to coalesce, reducing the effective interfacial mass transfer area. One important assumption of the model developed is that bubble coalescence is negligible and that all the bubbles have the same interfacial area and retain a single size throughout the reactor. The catalyst particles, however, cause deviations from these assumptions. Nevertheless, since operations are in the laminar regime and the superficial gas velocities are relatively low, significant deviations are not likely to occur.

The effect of velocity on the syngas conversion is more pronounced at lower than at higher catalyst loadings. This is due to the interplay of mass transfer and reaction kinetics. Note that for each catalyst loading given in Figure 7, an increase in velocity leads to a corresponding increase in reactor height. Thus in effect, there would be more catalyst in the reactor at higher velocities to maintain a constant catalyst loading.

**Variation in Reaction Temperature**

The effects of temperature on the FT process were simulated within a range of 240 °C to 270 °C within which the reactions are known to be carried out. The input parameters used are shown in Table 7 and the results obtained from the simulations in Figure 8. An increase in temperature generally leads to an increase in the conversion of syngas. This is primarily due to an increase in the kinetic rate constants of both the FT and WGS reactions. Since higher temperatures give higher conversions for a given reactor throughput, higher gas contractions are a consequence of this. The model predicts an initial slight increase and then a slight decrease in the WGS efficiency. This could in large part be due to the relative rates of the FT and WGS reactions as the temperature increases.

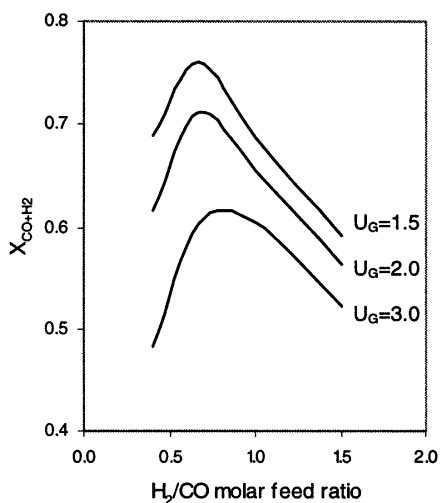


Figure 9a. Effect of the H<sub>2</sub>/CO inlet ratio on syngas conversion

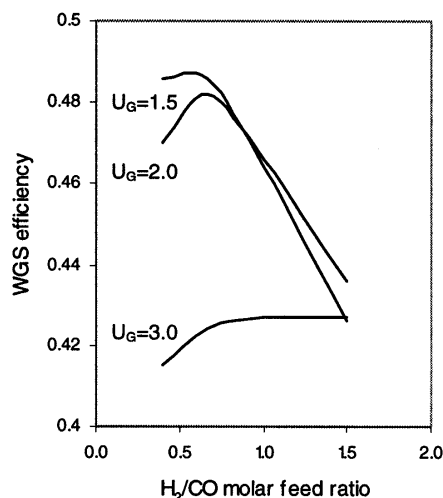


Figure 9b. Effect of the H<sub>2</sub>/CO inlet ratio on WGS efficiency

### Variation in Feed Composition

When iron-based catalysts are employed for the FT process, the feed gas composition becomes a very important parameter, since iron catalysts are active towards the WGS reaction. Due to the fact that H<sub>2</sub> is produced by the WGS reaction, a determination of the optimum amount of H<sub>2</sub> needed in the feed gas is necessary. Simulations were run in which the H<sub>2</sub>/CO inlet ratios were set at 0.4, 0.67, 1.0 and 1.5. Each of these feed ratios was simulated for the gas superficial velocities of 1.5, 2.0 and 3.0 cm/s. The feed was kept at 90 % syngas (CO and H<sub>2</sub>) and 10 % N<sub>2</sub>. Other input parameters can be seen in Table 7. Figure 9a clearly shows that the optimum feed ratio of H<sub>2</sub> to CO in the feed is about 0.67 as the highest syngas conversion is obtained here irrespective of the feed velocity within the range used. This is also the theoretical optimum. Lower and higher H<sub>2</sub>/CO ratios give lower conversions. At low H<sub>2</sub>/CO feed ratios (say H<sub>2</sub>/CO = 0.4), there is much less H<sub>2</sub> than is required. Thus H<sub>2</sub> conversion is very high as studies with the model revealed. However, due to the excess of CO, its conversion is low. At the optimum feed ratio, there is still a deficit of H<sub>2</sub> for the FT reaction. However, H<sub>2</sub>O produced by the FT reaction reacts with CO in the WGS to produce more H<sub>2</sub>. As can be seen from Figure 9b, the extent of WGS is highest around the optimum feed ratio (i.e. an H<sub>2</sub>/CO inlet ratio of ~0.67).

### Variation of CO<sub>2</sub> Composition in the Feed

CO<sub>2</sub> inhibits the FT process through the reverse WGS reaction. Yates and Satterfield (1989) have stated that this inhibition is actually due to inhibition by H<sub>2</sub>O (H<sub>2</sub>O being formed by the reverse WGS reaction in which CO<sub>2</sub> reacts with H<sub>2</sub>). Model simulations were run using the input data shown in Table 7 with the feed set at 60 % syngas while the remaining 40 % was either pure N<sub>2</sub> or a mixture of N<sub>2</sub> and CO<sub>2</sub>. The H<sub>2</sub>/CO ratio of the feed was set at 0.5, 0.67, 1.0 and 1.5. For each feed ratio, simulations were run in which the volumetric

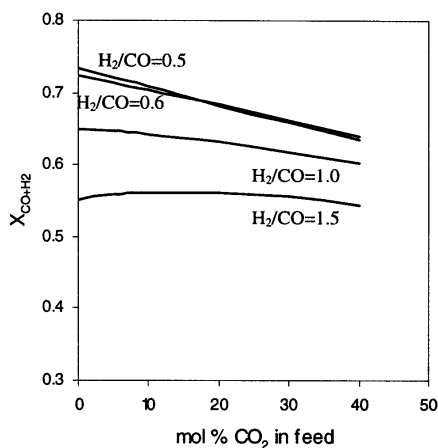


Figure 10a. Effect of CO<sub>2</sub> on syngas conversion

amount of CO<sub>2</sub> in the feed was 0, 5, 10, 20, 30 and 40 vol %.

Figures 10a and 10b show that an increase in the amount of CO<sub>2</sub> leads to a decrease in both the syngas conversion and the WGS efficiency of the process. The higher WGS activity at lower H<sub>2</sub>/CO feed ratios in comparison to higher ratios is due to the fact that in the former, very little H<sub>2</sub>O is formed by the FT reaction, while in the latter a significant amount of H<sub>2</sub>O can be formed. When the H<sub>2</sub>/CO inlet ratio is low, the concentration of H<sub>2</sub>O in the reactor is also low because the H<sub>2</sub>O produced by the FT reaction quickly reacts with CO via WGS to produce the H<sub>2</sub> needed in the FT reaction. This was revealed from studies on the slurry phase concentration profile obtained from the model. At high H<sub>2</sub>/CO feed ratios, more H<sub>2</sub>O is produced in the FT reaction than can be consumed by the WGS reaction. When this happens, H<sub>2</sub>O begins to inhibit the process. In a nutshell, CO<sub>2</sub> inhibition is intertwined with that of H<sub>2</sub>O.

### Mass Transfer and Reaction Kinetic Studies

Mass transfer resistance in the slurry FT process may reside in the gas phase, liquid phase or liquid–solid interface. Using Equations (29), (30) and (31), it was observed that for superficial feed velocities in the range of 1 to 6 cm/s, over 98% of all resistance to mass transfer for all components resided exclusively in the liquid film of the gas–liquid interface. Thus, gas film and liquid–solid interface resistances were neglected in developing the model as can be seen in Equations (16) and (17).

$$(\beta_G)_i = \frac{1}{m_i (k_G a)_i} \left( \frac{1}{m_i (k_G a)_i} + \frac{1}{(k_L a)_i} + \frac{1}{(k_s a_p)_i} \right)^{-1} \quad (29)$$

$$(\beta_L)_i = \frac{1}{(k_L a)_i} \left( \frac{1}{m_i (k_G a)_i} + \frac{1}{(k_L a)_i} + \frac{1}{(k_s a_p)_i} \right)^{-1} \quad (30)$$

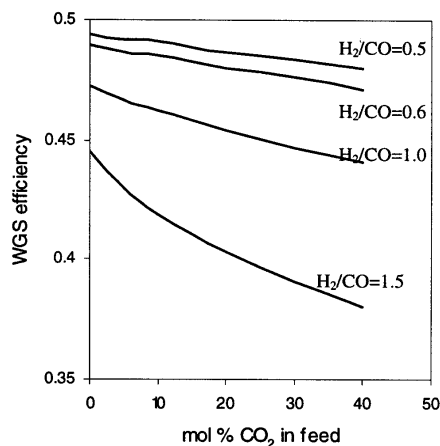


Figure 10b. Effect of CO<sub>2</sub> on WGS efficiency

$$(\beta_s)_i = \frac{1}{(k_s a_p)_i} \left( \frac{1}{m_i (k_G a)_i} + \frac{1}{(k_L a)_i} + \frac{1}{(k_s a_p)_i} \right)^{-1} \quad (31)$$

With mass transfer resistance known to reside at the liquid-side of the gas-liquid interface, there are then two resistances that affect the FT process: gas-liquid mass transfer and reaction kinetics. If mass transfer and chemical reaction occur in series (as will be verified later), they can be added thus for H<sub>2</sub> and CO:

$$\frac{1}{K_{H_2}} = \frac{1}{(k_L a)_{H_2}} + \frac{1}{k_{o,H_2}} \quad (32)$$

$$\frac{1}{K_{CO}} = \frac{1}{(k_L a)_{CO}} + \frac{1}{k_{o,CO}} \quad (33)$$

where k<sub>o,H<sub>2</sub></sub> and k<sub>o,CO</sub> are the overall kinetic rate constants for H<sub>2</sub> and CO, based on pseudo-first order reactions for both reactants. The pseudo-first order reactions for H<sub>2</sub> and CO are given by:

$$2R_{FT} - R_{WGS} = k'_{o,H_2} C_{H_2} \quad (34)$$

$$R_{FT} + R_{WGS} = k'_{o,CO} C_{CO} \quad (35)$$

And, k<sub>o,H<sub>2</sub></sub> and k<sub>o,CO</sub> are related to the pseudo-first order rate constants in Equations (34) and (35) by the expressions:

$$k_{o,H_2} = k'_{o,H_2} w_{cat} / V_L \quad (36)$$

$$k_{o,CO} = k'_{o,CO} w_{cat} / V_L \quad (37)$$

where V<sub>L</sub> is the volume of liquid in the reactor and w<sub>cat</sub>, the weight of catalyst particles. The relative extent of gas-liquid mass transfer resistance in the FT process becomes:

$$\beta_{H_2} = \frac{\frac{1}{(k_L a)_{H_2}}}{\frac{1}{(k_L a)_{H_2}} + \frac{1}{k_{o,H_2}}} \quad (38)$$

$$\beta_{CO} = \frac{\frac{1}{(k_L a)_{CO}}}{\frac{1}{(k_L a)_{CO}} + \frac{1}{k_{o,CO}}} \quad (39)$$

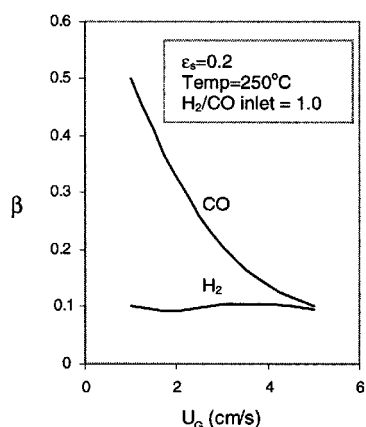


Figure 11. Effect of velocity on the relative mass transfer limitation

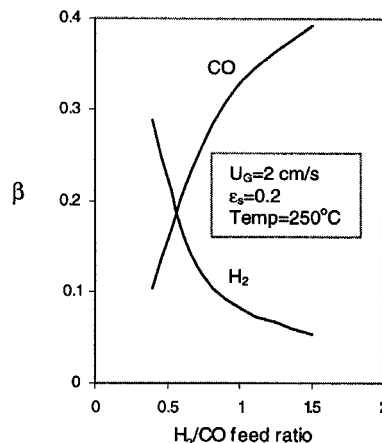


Figure 12. Effect of the inlet feed ratio on the relative mass transfer limitation

The effects of feed gas velocity, temperature, inlet feed ratio and catalyst loading on the relative mass transfer resistance were studied, using the data in Table 7. Within the operating conditions specified for Figure 11, the CO<sub>2</sub> relative resistance to mass transfer decreases with an increase in the feed gas velocity. This therefore means that at higher gas velocities the reaction kinetics play a more significant role than mass transfer in determining the rate of the process. The very low H<sub>2</sub> mass transfer resistance has to do with the fact that H<sub>2</sub> is produced in the slurry phase via WGS and not because it easily diffuses from the gas to the liquid phase. The H<sub>2</sub>/CO ratio used in the simulation was 1.0. There is therefore less H<sub>2</sub> than the amount required stoichiometrically and this would in turn favor the WGS reaction, which makes H<sub>2</sub> readily available in the slurry phase. However, as shown in Figure 12, for very low H<sub>2</sub>/CO inlet ratios, not enough H<sub>2</sub> can be produced in the slurry phase and H<sub>2</sub> mass transfer resistance becomes dominant. Since the rates of FT and WGS reactions increase with temperature, the effects of mass

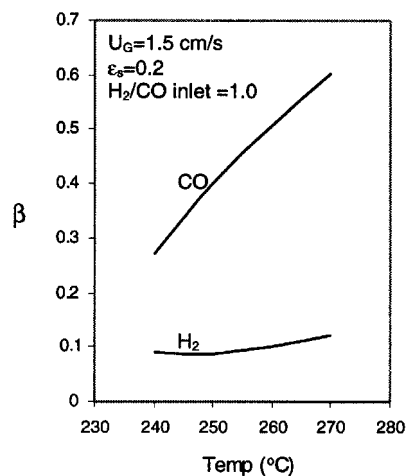


Figure 13. Effect of temperature on the relative mass transfer limitation

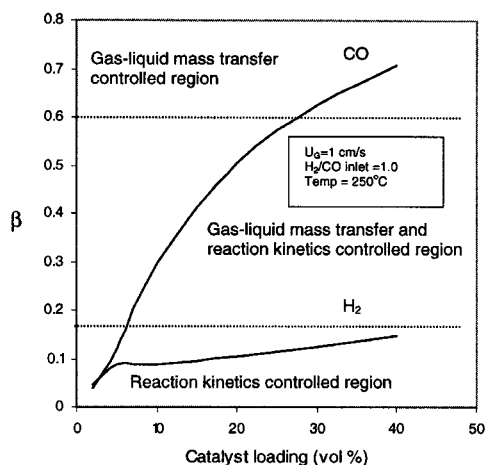


Figure 14. Effect of catalyst concentration on the relative mass transfer resistance for a gas velocity of 1 cm/s

transfer are more severe at high temperatures as shown in Figure 13. Satterfield and Huff (1980) reached the same general conclusion though their model utilized a first-order rate expression for the FT reaction and ignored the WGS reaction. Therefore, it could not discriminate between  $H_2$  and CO mass transfer resistances. Our model clearly shows the need for incorporating both the FT and WGS reactions to clearly understand how mass transfer affects  $H_2$  and CO.

Figure 14 shows that at low catalyst concentrations (less than 10 vol %), the laminar FT process is largely limited by reaction kinetics. As the catalyst concentration increases, both kinetics and mass transfer become significant in determining the rate of the reaction. At high catalyst concentrations, gas-liquid mass transfer becomes more significant than chemical kinetics in determining the rate of the process. The results in Figure 14 have been reproduced for higher gas velocities (3 to 5 cm/s). At higher velocities, the effects of mass transfer resistance are less pronounced. Similar results presented in Figure 14 have also been reported (Inga and Morsi, 1996) for an industrial sized reactor, operating in turbulent regime. Correlating the laminar flow results presented in this report to that, it shows that depending on the operating conditions, both gas-liquid mass transfer and reaction kinetics affect the iron-catalyzed FT process. The fact that both gas-liquid mass transfer and reaction kinetics do affect the reaction with both being rather significant under usual operating conditions in the laminar flow process means that both mass transfer and reaction occur in series. Had chemical reaction been much faster than mass transfer, this assumption would not have been valid.

## CONCLUSIONS

A mathematical model was developed for an iron-catalyzed laminar flow Fischer-Tropsch reactor and a comparison made to other similar models in the literature. Novel concepts about the model developed

include its ability to predict the extent of gas contraction, a key factor that determines syngas conversion. Two sets of experiments bordering on the FT process were also carried out. Based on the work done, the following conclusions were reached:

1. With catalyst loadings of between 6 and 9 vol% of the gas-free slurry phase, moderate syngas conversions can be obtained for the particular catalyst particles used when operating at very low superficial velocities.

2. Biosyngas obtained from the gasification of biomass can be employed in the FT process for the production of liquid fuels and waxes.  $CO_2$  present in the biosyngas does have a noticeable inhibiting effect on the FT process due to the formation of water as the WGS equilibrium is shifted.

3. The mathematical model developed for the reactor is valid to describe the qualitative performance of the reactor. Values of the FT and WGS rate constants used in the model are critical in obtaining accurate quantitative model predictions of the performance of the reactor. It is certain from the investigations that the catalyst activity changes with time on stream.

4. Gas-liquid mass transfer was determined to be the only significant mass transfer limitation in the FT process. Both gas-liquid mass transfer and reaction kinetics affect the rate of the process in the laminar regime of operation. At extremely low catalyst loading, kinetics limit the reaction, while at high catalyst loading, mass transfer limitation was found to be dominant. For  $H_2/CO$  inlet feed ratios greater than 0.67, the CO mass transfer limitation is greater than that of  $H_2$ .

## ACKNOWLEDGEMENT

The authors would like to thank the technicians at the Energy Research Center of the Netherlands for their assistance in fitting and operating the slurry bubble column reactor employed in this study.

## NOMENCLATURE

A	reactor cross-sectional area ( $m^2$ )
a	gas bubble specific surface ( $m^2/m^3$ )
$a_p$	catalyst specific surface ( $m^2/m^3$ )
$Bo_G$	gas phase Bodenstein number
$Bo_L$	liquid (slurry) phase Bodenstein number
$C_{G,i}^{in}$	gas phase concentration of component i into the reactor model gas phase CISTR ( $mol/m^3$ )
$C_{G,i}^{out}$	gas phase concentration of component i out of the reactor model gas phase CISTR ( $mol/m^3$ )
$C_{L,i}^{in}$	liquid phase concentration of component i into the reactor model slurry phase CISTR ( $mol/m^3$ )
$C_{L,i}^{out}$	liquid phase concentration of component i out of the reactor model slurry phase CISTR ( $mol/m^3$ )
$D_{G,i}$	gas phase diffusion coefficient of component i in the mixture of gases ( $m^2/s$ )
$D_L$	liquid phase dispersion coefficient ( $m^2/s$ )
$D_{L,i}$	diffusion coefficient of component i into the liquid phase ( $m^2/s$ )
$d_b$	gas bubble diameter (m)
$d_t$	reactor diameter (m)

E <sub>FT</sub>	Fischer–Tropsch reaction activation energy (kJ/mol)
E <sub>WGS</sub>	water gas shift reaction activation energy (kJ/mol)
eq	equilibrium condition
g	gravitational acceleration (m/s <sup>2</sup> )
H	reactor dispersion height (m)
k <sub>o,H<sub>2</sub></sub>	corrected pseudo first order rate constant for H <sub>2</sub> (s <sup>-1</sup> )
k <sub>o,CO</sub>	corrected pseudo first order rate constant for CO (s <sup>-1</sup> )
(k <sub>G<i>i</i></sub> ) <sub>i</sub>	volumetric gas phase mass transfer coefficient of component <i>i</i> (s <sup>-1</sup> )
(k <sub>L<i>i</i></sub> ) <sub>i</sub>	volumetric liquid phase mass transfer coefficient of component <i>i</i> (s <sup>-1</sup> )
(k <sub>s<i>a<i>p</i></i></sub> ) <sub>i</sub>	volumetric mass transfer coefficient through the liquid–solid interface of component <i>i</i> (s <sup>-1</sup> )
m <sub>i</sub>	solubility or partition coefficient, [(C <sub>G,<i>i</i>)<sub>eq</sub>/(C<sub>L,<i>i</i>)<sub>eq</sub>]</sub></sub>
n	number of vessels (tanks–in–series model), Equation (25)
n <sub>G</sub>	number of gas phase CISTRs used to model the reactor
n <sub>L</sub>	number of slurry phase CISTRs used to model the reactor
P <sub>i</sub>	partial pressure of component <i>i</i> (MPa)
R	gas constant (8.314x10 <sup>-6</sup> MPa m <sup>3</sup> mol <sup>-1</sup> K <sup>-1</sup> )
R <sub>FT</sub>	rate of Fischer–Tropsch reaction (mol/kg <sub>cat</sub> .s)
R <sub>WGS</sub>	rate of water gas shift reaction (mol/kg <sub>cat</sub> .s)
T	reaction temperature (K)
U <sub>G</sub>	superficial gas velocity along the reactor (m/s)
U <sub>G</sub> <sup>in</sup>	superficial gas velocity into the reactor model gas phase CISTR (m/s)
U <sub>G</sub> <sup>inlet</sup>	superficial gas velocity into the reactor (m/s)
U <sub>G</sub> <sup>out</sup>	superficial gas velocity out of the reactor model gas phase CISTR (m/s)
U <sub>L</sub> <sup>n</sup>	superficial slurry velocity into the reactor model slurry phase CISTR (m/s)
U <sub>L</sub> <sup>out</sup>	superficial slurry velocity out of the reactor model slurry phase CISTR (m/s)
V <sub>L</sub>	volume of liquid in the reactor (m <sup>3</sup> )
w <sub>cat</sub>	weight of catalyst particles in the reactor (kg)
X	gas conversion, first order reaction, Equation
X <sub>H<sub>2</sub>+CO</sub>	syngas conversion

#### Kinetic Parameters

a	adsorption coefficient of CO (MPa <sup>-1</sup> )
b	adsorption coefficient of H <sub>2</sub> (MPa <sup>-1</sup> )
k <sub>FT</sub>	Fischer–Tropsch reaction rate constant (mol kg <sup>-1</sup> s <sup>-1</sup> MPa <sup>-1.5</sup> )
k <sub>WGS</sub>	water gas shift reaction rate constant (mol kg <sup>-1</sup> s <sup>-1</sup> )
K	adsorption coefficient of H <sub>2</sub> O
K <sub>p</sub>	equilibrium constant of the WGS reaction

#### Greek symbols

a <sub>c</sub>	gas contraction factor
(β <sub>G</sub> ) <sub>i</sub>	relative extent of the gas–film mass transfer resistance at the gas–liquid interface to total mass transfer resistance for component <i>i</i>
(β <sub>L</sub> ) <sub>i</sub>	relative extent of the liquid–film mass transfer resistance at the gas–liquid interface to the total mass transfer resistance for component <i>i</i>
(β <sub>S</sub> ) <sub>i</sub>	relative extent of the solid–film mass transfer resistance at the liquid–solid interface to the total mass transfer resistance for component <i>i</i>
β <sub>H<sub>2</sub></sub>	relative extent of the mass transfer resistance to the total resistance with respect to H <sub>2</sub>
β <sub>CO</sub>	relative extent of the mass transfer resistance to the total resistance with respect to CO
d	gas film thickness (m)
Dz	height of one gas phase CISTR in the reactor model (m)
DH	height of one slurry phase CISTR in the reactor model (m)

eg	gas hold-up
eL	liquid hold-up
es	solids hold-up (catalyst loading)
hL	dynamic liquid viscosity (Pa.s or cP as applicable)
rg	gas density (kg/m <sup>3</sup> )
rL	liquid density (kg /m <sup>3</sup> )
sL	surface tension of the liquid phase (N/m)
nL	kinematic viscosity of the liquid phase (m <sup>2</sup> /s)
w <sub>i</sub>	stoichiometric coefficient of component <i>i</i> in the rate expression

#### REFERENCES

- [1] Akita, K., and Yoshida, F. (1974). Bubble Size, Interfacial Area, and Liquid–Phase Mass Transfer Coefficient in Bubble Columns, *Ind. Eng. Chem. Proc. Des. Dev.*, **13**, 84–91
- [2] Anderson, R.B. (1984). *The Fischer–Tropsch Synthesis*, Academic Press Inc
- [3] Beenackers, A.A.C.M., and van Swaaij, W.P.M. (1993). Mass Transfer in Gas–Liquid Slurry Reactors, *Chem. Eng. Sci.*, **48**, 3109–3139
- [4] Boerrigter, H., Den Uil, H., and Calis, H.–P. (2002). Green Diesel from Biomass via Fischer–Tropsch synthesis: New Insights in Gas Cleaning and Process Design, Paper presented at Pyrolysis and Gasification of Biomass and Waste, Expert Meeting, 30 September – 1 October, Strasbourg, France
- [5] Bukur, D.B. (1983). Some comments on models for Fischer–Tropsch reaction in slurry bubble column reactors, *Chem. Eng. Sci.*, **38**, 441–446
- [6] Bukur, D.B. and Zimmerman, W.H. (1987). Modelling of bubble column slurry reactors for multiple reactions, *AIChE Journal*, **33**, 1197–12–0
- [7] Bukur, D.B., Lang, X., Rossin, J.A., Zimmerman, W.H., Rosynek, M.P., Yeh, E.B., Li, C. (1989). Activation Studies with a Promoted Precipitated Iron Fischer–Tropsch Catalyst, *Ind. Eng. Chem. Res.*, **28**, 1130–1140
- [8] Bukur, D.B., Nowicki, L., Manne, R.K., and Lang, X. (1995). Activation Studies with a Precipitated Iron Catalyst for Fischer–Tropsch Synthesis II. Reaction Studies, *Journal of Catalysis*, **155**, 366–375
- [9] Calderbank, P.H., Evans, F., Farley, R., Jepson, G., and Poll, A. (1963). Rate processes in the catalyst–slurry Fischer–Tropsch reaction, *Catal. in Practice*, 66–74
- [10] Davis, B.H., O'Brien, R.J., Raje, A., Spicer, R.L., Xu, L., Bao, S., and Lambert, S. (1998). Technology Development for Iron Fischer–Tropsch Catalysts, U.S. Dept. of Energy Study, Kentucky Research Foundation
- [11] De Swart, J.W.A., Krishna, R., and Sie, S.T. (1997). Selection, design and scale up of the Fischer–Tropsch slurry reactor, *Surface Science and Catalysis*, **107**, 213–218
- [12] Deckwer, W.–D., Serpemen, Y., Ralek, M., and Schmidt, B. (1982). Modeling the Fischer–Tropsch synthesis in the slurry phase, *Ind. Eng. Chem. Process Des. Dev.*, **21**, 231–241
- [13] Deckwer, W.–D., Kokuun, R., Sanders, E., and Ledakowicz, S. (1986). Kinetic Studies of Fischer–Tropsch Synthesis on Suspended Fe/K Catalyst–Rate Inhibition by CO<sub>2</sub> and H<sub>2</sub>O, *Ind. Eng. Chem. Process Des. Dev.*, **25**, 643–649
- [14] Deckwer, W.–D. (1992). *Bubble Column Reactors*, John Wiley and Sons, New York
- [15] Dry, M.E. (1981). *The Fischer–Tropsch Synthesis*, in J.R. Anderson and M. Boudart, editors, *Catalysis–Science and Technology*, Vol. 1, Springer–Verlag, New York, 159–255
- [16] Fogler, H.S. (1999). *Elements of Chemical Reaction Engineering*, 3rd edition, Prentice Hall, New Jersey

- [17] Huff, G.A., and Statterfield, C.N. (1984). Evidence for two chain growth probabilities on iron catalysts in the Fischer–Tropsch synthesis, *Journal of Catalysis*, **85**, 370–379
- [18] Inga, J.R., and Morsi, B.I. (1996). A novel approach for the assessment of the rate-limiting step in Fischer–Tropsch slurry process, *Energy and Fuels*, **10**, 566–572
- [19] Krishna, R., and Ellenberger, J. (1996). Gas Holdup in Bubble Column Reactors Operating in the Churn–Turbulent Flow Regime, *AIChE Journal*, **42**(9), 2627–2634
- [20] Krishna, R., De Swart, J.W.A., Ellenberger, J., Martina, G.B., and Maretto, C. (1997). Gas Holdup in Slurry Bubble Column Reactors: Effect of Column Diameter and Slurry Concentrations, *AIChE Journal*, **43**(2), 311–316
- [21] Krishna, R., and Maretto, C. (1999). Modelling of a bubble column slurry reactor for Fischer–Tropsch synthesis, *Catalysis Today*, **52**, 279–289
- [22] Kuo, J.C.W. (1983). Slurry Fischer–Tropsch/Mobil two stage process of converting syngas to high octane gasoline, Final report DOE–PC–3022–10, DOE
- [23] Ma, W.P., Ding, Y.J., Vazquez, V.H.C. and Bukur, D.B. (2004). Study on the catalytic performance and attrition strength of the Ruhrchemie catalyst for the Fischer–Tropsch synthesis in a stirred tank slurry reactor, *Applied Catalysis A–General*, **268**, 99–108
- [24] Prakash, A. (1994). On the effects of syngas composition and water–gas–shift reaction rate on FT (Fischer–Tropsch) synthesis over iron based catalyst in a slurry reactor, *Chem. Eng. Commun.*, **128**, 143–158
- [25] Reid, R.C., Prausnitz, J.M., and Poling, B.E. (1987). *The Properties of Gases and Liquids*, 4th edition, McGraw–Hill, New York
- [26] Satterfield, C.N., and Huff, G.A. (1980). Effects of mass transfer on Fischer–Tropsch synthesis in slurry reactors, *Chem. Eng. Sci.*, **35**, 195–202
- [27] Saxena, S.C., Rosen, M., Smith, D.N., and Ruether, J. A. (1986). Mathematical Modeling of Fischer–Tropsch Slurry Bubble Column Reactors, *Chem Eng Commun.*, **40**, 97–151
- [28] Saxena, S.C. (1995). Bubble Column Reactors and Fischer–Tropsch Synthesis, *Catal. Rev.– Sci. Eng.*, **37**(2), 227–309
- [29] Shah, Y., Kelkar, B., Godbole, S., and Deckwer, W. –D. (1982). Design parameters estimation for bubble column reactors, *AIChE Journal*, **28**, 353
- [30] Shell International (2001) *Energy Needs, Choices and Possibilities – Scenarios to 2050*
- [31] Shen, W.J., Zhou, J.L., and Zhang, B.J. (1994). Kinetics of Fischer–Tropsch synthesis over precipitated iron catalyst, *J. Nat. Gas Chem*, **4**, 385–400
- [32] Stenger, H.G., and Satterfield, C.N. (1985). Effects of sulfur poisoning of a reduced fused magnetite catalyst in the Fischer–Tropsch synthesis, *Ind. Eng. Chem. Process Des. Dev.*, **24**, 415–420
- [33] Stern, D., Bell, A.T., and Heinemann, H. (1985). A theoretical model for the performance of bubble–column reactors used for Fischer–Tropsch synthesis, *Chem. Eng. Sci.*, **40**(9), 1665–1677
- [34] Van der Laan, G.P. (1999). Kinetics, Selectivity and Scale Up of the Fischer–Tropsch Synthesis, PhD thesis, Rijksuniversiteit Groningen, The Netherlands
- [35] Van der Laan, G.P., Beenackers, A.A.C.M., and Krishna, R. (1999). Multicomponent reaction engineering model for Fe–catalyzed Fischer–Tropsch synthesis in a commercial scale slurry bubble column reactors, *Chem. Eng. Sci.*, **54**, 5013–5019
- [36] Yates, I.C., and Satterfield C.N. (1989). Effects of Carbon Dioxide on the Kinetics of the Fischer–Tropsch Synthesis on Iron Catalysts, *Ind. Eng. Chem. Res.*, **28**, 9–12
- [37] Zimmerman, W.H. and Bukur, D.B. (1991). On the use of approximate velocity profiles for modeling multiphase reactors, *Can. J. Chem. Eng.*, **69**, 325–331

## IZVOD

### ISPITIVANJE FISHER–TROPSCHE SINTEZE SA SUSPENDOVANIM GVOŽDEM KAO KATALIZATOROM U LAMINARNOM KOLONSKOM REAKTORU

(Naučni rad)

C.O. Vandu<sup>1</sup>, A.B.M. Heesink<sup>1</sup>, G.F. Versteeg<sup>1</sup>, H. Boerrigter<sup>2</sup>

<sup>1</sup>Fakultet za prirodne nauke i tehnologije, Univerzitet Twente, Enschede, Holandija

<sup>2</sup>Holandski centar za energetska ispitivanja, Paten, Holandija

Ispitivana je Fischer–Tropsch (F–T) sinteza u laminarnom kolonskom reaktoru. Prethodno su realizovana hidrodinamička ispitivanja u istom tipu reaktora na hladno. Na osnovu kinetičkih podataka za gvožđe kao katalizator razvijen je matematički model F–T procesa. On je omogućio isračunavanje smanjenja (kontrakcije) zapremine gasovite reakcione smeše tokom reakcije. Na osnovu šest eksperimenata potvrđena je valjanost definisanog modela pri čemu su podešavani parametri modela i definisan uticaj aktivnosti katalizatora tokom F–T sinteze. Proučavan je uticaj jednog broja parametara modela na F–T sintezu.

Ključne reči: Fisher–Tropsch sinteza, Gvožđe kao katalizator, Barbofažna kolona sa suspendovanim katalizatorom, Biomasa, Biosintezni gas.